molecular pharmaceutics

pubs.acs.org/molecularpharmaceutics

Communication

Synthesis and Biological Evaluation of ^{131}I-Risedronate with Bone Targeting Activity

Zehui Lin,[‖] Wangxi Hai,[‖] Pengfei Pan, Jin-Hong Lin,* Biao Li,* and Ji-Chang Xiao*

Cite This: *Mol. Pharmaceutics* 2025, 22, 3508−3514

Read Online

ACCESS | Metrics & More | Article Recommendations | Supporting Information

ABSTRACT: Current radiopharmaceuticals for treating bone metastatic tumors have various limitations. We focus on developing a universal, economical, efficient, and safe novel radiopharmaceutical for bone metastasis treatment. ^{131}I is a well-established medical radionuclide commonly used for both treatment and diagnosis. Risedronate exhibits strong bone-targeting properties with moderate bone retention. This study explored the combination of these two components and evaluated its biological properties in animal experiments. Based on the experimental results, ^{131}I-risedronate demonstrated high bone-targeting efficiency, low uptake in nontarget organs, and rapid clearance. Notably, at 3 days postadministration, significant bone retention was observed, indicating its potential for sustained therapeutic effects. Additionally, its biodistribution and therapeutic effect can be effectively monitored by SPECT/CT imaging.

KEYWORDS: *Radiopharmaceuticals, Radiochemistry, Bone metastasis, Iodine-131, ^{131}I-risedronate*

1. INTRODUCTION

Bone is one of the most common sites for malignant tumor metastasis, and various radiopharmaceuticals have been developed for the clinical diagnosis and treatment of bone metastasis.[1,2] Current treatment strategy is primarily palliative, aiming to alleviate patient pain by precisely targeting the tumor site with drugs.[3] Existing radiopharmaceuticals can be divided into two main categories: the first category includes metal ion-based radiopharmaceuticals, represented by strontium-89 chloride and radium-223 chloride, which rely on the inherent bone affinity of metal ions to achieve bone accumulation.[4,5] While they exhibit certain therapeutic effects, their lack of targeting selectivity can lead to adverse side effects. The second category includes bisphosphonate-conjugated radiopharmaceuticals, such as ^{153}Sm-EDTMP, ^{186}Re-HEDP, and ^{177}Lu-DOTA-IBA.[6−8] These drugs leverage the high affinity of bisphosphonates for bone tissue to enhance the precision of radionuclide delivery, significantly reducing off-target organ exposure. However, these drugs face production barriers—such as the need for reactor irradiation for ^{186}Re production and the difficulty in extracting ^{223}Ra, leading to supply shortages in some countries. Additionally, the limited efficacy of current drugs and multiple clinical application restrictions have severely hindered their widespread adoption.

Given the current technological bottlenecks, developing novel radiopharmaceuticals that are universal, cost-effective, and efficient has become a critical research direction in the treatment of bone metastases. As a classic representative of the radionuclide diagnostic and therapeutic system, ^{131}I has demonstrated unique dual advantages in clinical applications.[9] Its mature production process and lower usage costs make it an important choice in nuclear medicine, particularly where standardized clinical pathways have already been established for thyroid disease diagnosis and treatment.[10,11] The radiological properties of ^{131}I provide a foundation for its diverse applications: Its 8-day half-life ensures continuous radioactivity while avoiding excessive biological retention risks. The β radiation (606 keV) released during decay has a tissue penetration depth of 1−2 mm, effectively killing tumor cells. Meanwhile, the accompanying γ radiation (364 keV) enables high-quality SPECT/CT imaging, facilitating visual monitoring of the treatment process. However, its specific application in the diagnosis and treatment of bone metastatic tumors remains unexplored.

Risedronate is one of the third-generation bisphosphonates with strong bone affinity.[12,13] Risedronate can strongly coordinate with calcium ions in hydroxyapatite (HAP) of bone tissue through its bisphosphonate structure. After injection, it rapidly accumulates on the bone surface, particularly in metabolically active bone regions such as the vertebrae, femur, and pelvis, where increased exposure of calcium sites facilitates drug binding.[14,15] Bone metastases enhance local bone turnover by secreting cytokines (e.g., PTHrP, IL-6), which activate osteoclasts and accelerate bone resorption,[16,17] thereby increasing HAP exposure and promoting further accumulation of risedronate at these sites. In contrast, soft tissues lack HAP and thus provide no binding sites. As bone metastases are more metabolically active than normal bone regions, the greater the bone turnover and calcium ion exposure, the higher the selective accumulation of risedronate in these lesions. Additionally, the pyridine ring of

Received: March 4, 2025
Revised: April 22, 2025
Accepted: April 23, 2025
Published: May 1, 2025

https://doi.org/10.1021/acs.molpharmaceut.5c00300
Mol. Pharmaceutics 2025, 22, 3508−3514

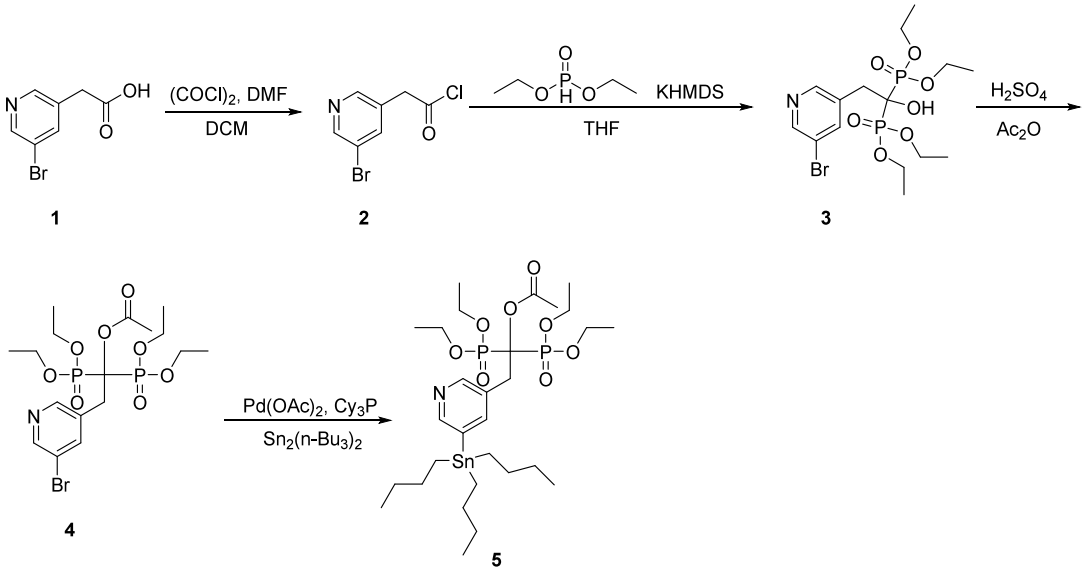

Figure 1. Synthesis of 1,1-bis(diethoxyphosphoryl)-2-[5-(tributylstannyl)pyridin-3-yl]ethyl acetate.

risedronate has considerable steric hindrance, and can enhance binding to HAP through $\pi-\pi$ stacking, hydrogen bonding, and electrostatic interactions. The pyridine-containing structure not only contributes to a moderate retention time, but also confers significantly higher bone affinity compared to earlier generations of bisphosphonates.[18]

Up to now, the research on ^{131}I-based drugs has expanded to other diseases beyond thyroid disorders, such as neuroendocrine tumors (^{131}I-MIBG)[19] and non-Hodgkin lymphoma (^{131}I-Tositumomab).[20] In this study, we labeled ^{131}I for the first time onto a bone-targeting drug, using ^{131}I-risedronate as an example, to investigate the potential of ^{131}I in the treatment of bone metastases. We hope that this molecule can carry ^{131}I to rapidly distribute to bone metastatic tumor sites and provide sustained radiotherapy effects over a period of time.

2. MATERIALS AND METHODS

2.1. General. All commercially available reagents and solvents are analytical or HPLC grade and used without purification. ^{1}H and ^{31}P spectra were obtained using an Agilent 400 MHz NMR spectrometer, and ^{13}C spectra were obtained using a Bruker 400 MHz NMR spectrometer. Mass data were obtained by Shimadzu LCMS-2020 with ESI as ion source in positive modes. HRMS data were obtained by Thermo Scientific Q Exactive HF Orbitrap-FTMS with ESI as ion source in positive modes. For HPLC and radio-HPLC an Agilent 1200 LC with an UV and a radio detector was used. ^{131}I was provided by China Isotope & Radiation Corporation (Beijing, China) as NaI aqueous solution. BALB/c mice were purchased from Sibeifu (Suzhou) Biotechnology Co., Ltd., with an animal license number SCXK (Su) 2022−0006. A gamma counter (Beijing PET Technology Co., Ltd., Model JC-2101) was used for counting measurements. The activity of ^{131}I was measured using a radioactivity meter (Beijing Tongxiang High Technology Development Co., Ltd., Model HD-175). Whole-body images were acquired using the MOLECUBES small animal single-photon emission computed tomography system (x-cube, γ-cube MOLECUBES, Belgium). The acquisition was performed in the prone position using a Lofthole collimator with a 10% energy window centered at a photopeak of 364.49 keV. All the animal experiments were approved by Laboratory Animal Ethics Committee of Ruijin Hospital, Shanghai Jiao Tong University School of Medicine.

2.2. Synthesis of Precursor. Figure 1

2.2.1. (5-Bromopyridin-3-yl)acetyl chloride. To a stirred mixture of compound **1** (2.00 g, 9.25 mmol) in dichloromethane (50 mL) was added oxalyl chloride (5 mL) at 0 °C under nitrogen atmosphere. The resulting mixture was stirred for 10 min at room temperature under nitrogen atmosphere. To the above mixture was added a few drops of *N*,*N*-dimethylformamide at room temperature. The resulting mixture was stirred for additional 1 h at room temperature. The reaction was monitored by LCMS. The resulting mixture was concentrated under reduced pressure to afford compound **2** (2.36 g, crude product) as a light yellow solid. The crude product was used in the next step directly without further purification.

2.2.2. Diethyl 2-(5-bromopyridin-3-yl)-1-(diethoxyphosphoryl)-1-hydroxyethylphosphonate. To a stirred mixture of diethyl phosphite (2.35g, 17.04 mmol) in tetrahydrofuran (100 mL) was added KHMDS (1 M in THF, 9.40 mL) dropwise at −78 °C under nitrogen atmosphere. The resulting mixture was stirred for 30 min at −78 °C under nitrogen atmosphere. The mixture was allowed to cool down to −100 °C. To the above mixture was added compound **2** (2 g, 8.52 mmol) at −100 °C. The resulting mixture was stirred for additional 5 h under 0 °C. The reaction was quenched with sat. ammonium chloride (aq.) at −30 °C. The mixture was allowed to warm up to room temperature. The resulting mixture was extracted three times with ethyl acetate. The combined organic layers were washed with brine, dried over anhydrous sodium sulfate. After filtration, the filtrate was concentrated under reduced pressure. The residue was purified by silica gel column chromatography, eluted with ethyl acetate/ethanol (5/1). The product was further purified by reversed-phase flash chromatography and concentrated under reduced pressure to afford compound **3** (0.64 g, 15.03%) as a brown oil. ^{1}H NMR (400 MHz, DMSO-d_6) δ 8.53 (d, J = 2.4 Hz, 1H), 8.43 (d, J = 2.0 Hz, 1H), 8.15 (s, 1H, introduced by HPLC), 7.95 (t, J = 2.0 Hz, 1H), 6.43 (s, 1H), 4.20−3.88 (m, 8H), 3.17 (t, J = 13.2 Hz, 2H), 1.43−1.06 (m, 12H). ^{31}P NMR (162 MHz, DMSO-

https://doi.org/10.1021/acs.molpharmaceut.5c00300
Mol. Pharmaceutics 2025, 22, 3508−3514

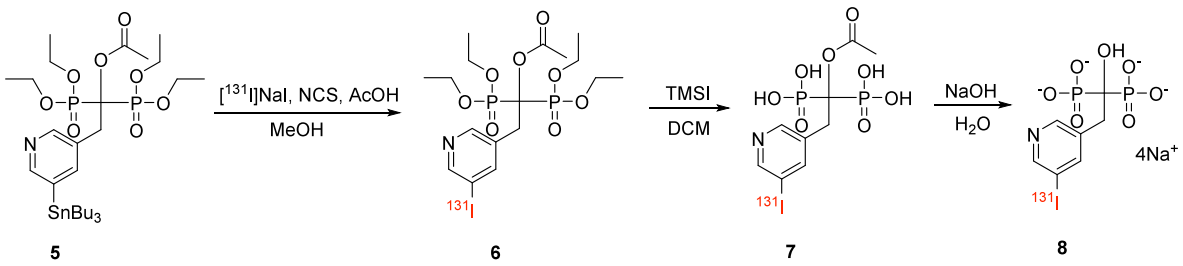

5 6 7 8

Figure 2. Radiolabeling of precursor and deprotection of ^{131}I-risedronate.

d_6) δ 18.79. MS (ESI) calculated for $C_{15}H_{27}BrNO_7P_2$ [M + H]$^+$ 474.04, found 473.95.

2.2.3. 2-(5-Bromopyridin-3-yl)-1,1-bis-(diethoxyphosphoryl)ethyl acetate. To a stirred mixture of compound **3** (0.64 g, 1.35 mmol) in acetic anhydride (5 mL) was added sulfuric acid (0.5 mL) at room temperature under nitrogen atmosphere. The resulting mixture was stirred at room temperature for 2 h under nitrogen atmosphere. The reaction was monitored by LCMS. The reaction was quenched by the addition of Water/Ice at 0 °C. The resulting mixture was extracted three times with dichloromethane. The combined organic layers were washed two times with 1 M hydrochloric acid (aq.) and sat. sodium bicarbonate, dried over anhydrous sodium sulfate. After filtration, the filtrate was concentrated under reduced pressure. The residue was purified by reversed-phase flash chromatography and concentrated under reduced pressure to afford compound **4** (0.54 g, 73.63%) as a yellow oil. ^{1}H NMR (400 MHz, DMSO-d_6) δ 8.59 (d, J = 2.4 Hz, 1H), 8.31 (d, J = 2.0 Hz, 1H), 7.79 (t, J = 2.0 Hz, 1H), 4.17−3.96 (m, 8H), 3.63−3.47 (m, 2H), 2.13 (s, 3H), 1.18 (q, J = 7.2 Hz, 12H). ^{31}P NMR (162 MHz, DMSO-d_6) δ 14.85. MS (ESI) calculated for $C_{17}H_{29}BrNO_8P_2$ [M + H]$^+$ 518.05, found 517.95.

2.2.4. 1,1-Bis(diethoxyphosphoryl)-2-[5-(tributylstannyl)-pyridin-3-yl]ethyl acetate. To a stirred mixture of compound **4** (0.54 g, 1.04 mmol) in 1,1,1,2,2,2-hexabutyldistannane (5 mL) were added tricyclohexyl phosphine (56 mg, 0.2 mmol) and $Pd(OAc)_2$ (22.4 mg, 0.1 mmol) at room temperature under nitrogen atmosphere. The mixture was purged by nitrogen. The resulting mixture was stirred at 110 °C for 40 min under nitrogen atmosphere. The reaction was monitored by LCMS. The mixture was allowed to cool down to room temperature. The residue was purified by silica gel column chromatography, eluted with ethyl acetate/ethanol (4/1) to afford compound **5** (152 mg, 20.10%) as a yellow oil. ^{1}H NMR (400 MHz, DMSO-d_6) δ 8.43−8.34 (m, 1H), 8.24 (d, J = 2.4 Hz, 1H), 7.61−7.47 (m, 1H), 4.14−3.92 (m, 8H), 3.58−3.43 (m, 2H), 2.10 (s, 3H), 1.60−1.39 (m, 6H), 1.33−1.23 (m, 6H), 1.17 (t, J = 7.2 Hz, 6H), 1.13−0.97 (m, 12H), 0.85 (t, J = 7.2 Hz, 9H). ^{31}P NMR (162 MHz, DMSO-d_6) δ 15.00. ^{13}C NMR (101 MHz, DMSO-d_6) δ 169.01, 153.71, 150.84, 145.45, 134.69, 130.53, 82.09 (t, J = 149.1 Hz), 63.14 (dt, J = 47.7, 3.3 Hz), 33.69, 28.49, 26.68, 20.95, 15.99 (dt, J = 5.9, 2.9 Hz), 13.47, 9.14. HRMS (ESI) calculated for $C_{29}H_{56}NO_8P_2Sn$ [M + H]$^+$ 728.2502, found 728.2498.

2.3. Radiolabeling with ^{131}I and the Subsequent Deprotection and Purification. To a stirred mixture of compound **5** (100 μg) in 0.1 mL methanol were added 400 μL of [^{131}I]NaI aqueous solution (20−40 mCi), 33 μL of methanol solution of NCS (3 mg/mL), and 20 μL of acetic acid. The resulting mixture was stirred at room temperature for 30 min. The residue was purified by Radio HPLC to afford compound **6** (17−32 mCi, radiation yield 80−85%). Compound **6** was enriched by using an HLB solid-phase extraction column and eluted with acetonitrile. The eluent was dried at 100 °C for 10 min and added 500 μL of DCM solution of TMSI (0.4 M). The resulting mixture was stirred at room temperature for 2 h. The residue was enriched by SCX cation exchange column, and the column was washed sequentially with 5 mL of ethanol and 5 mL of pure water. The product was eluted with 1 mL of 2 M NaOH solution. The mixture was heated the at 50 °C for 5 min and cooled down to room temperature. The pH of the solution was adjusted to neutral to afford ^{131}I-risedronate (compound **8**, radiation purity >99%) Figure 2.

2.4. In Vitro Stability. A volume of 500%μL of ^{131}I-risedronate solution (approximately 1%mCi) was mixed with an equal volume of human plasma in an anticoagulant centrifuge tube. The mixture was incubated at 37%°C in a thermostatic incubator. At predetermined time points (0, 1, 6, 12, and 24%h), 100%μL aliquots were withdrawn and mixed with 200%μL of acetonitrile to precipitate plasma proteins. The samples were then placed at − 20%°C for 10 min, followed by centrifugation at 10,000%rpm for 10 min. The supernatant was collected and subjected to radio-HPLC analysis.

2.5. In Vivo Biodistribution Testing. Normal BALB/c mice were randomly divided into four groups (n = 16, 1/2male, and 1/2 female). Each mouse was injected with a dose of 50−70 μCi of ^{131}I-risedronate, and the activity of ^{131}I was measured using a radioactivity meter. After ^{131}I-risedronate injection, at 1 h, 4 h, 1 day, and 3 days, the following organs were collected: blood, femur, muscle, intestine, stomach, heart and kidney, then weighed and measured in a gamma counter. The%ID/g was calculated for each organ of interest.

2.6. Micro SPECT/CT Imaging. Normal mice were injected intravenously with 50−70 μCi of ^{131}I-risedronate, and whole-body static bone scanning was performed with a micro SPECT/CT scanner at 1h, 4h, 1 day, and 3 days after injection. The MOLECUBES x-cube device acquisition parameters were as follows: tube voltage: 50 kV; tube current: 30 μA; exposure time: 3 min. The MOLECUBES γ-cube device acquired whole-body images for 20 min. The data acquired by the MOLECUBES x-cube were reconstructed using an iterative algorithm with a voxel size of 200 μm. The data acquired by the MOLECUBES γ-cube were reconstructed using the Maximum Likelihood Expectation Maximization (MLEM) algorithm with 50 iterations and a voxel size of 500 μm. Attenuation-corrected coronal, axial, and sagittal tomographic images and 3D MIP images were generated for data analysis.

https://doi.org/10.1021/acs.molpharmaceut.5c00300
Mol. Pharmaceutics 2025, 22, 3508−3514

3. RESULTS AND DISCUSSION

3.1. Syntheses of ^{131}I-Risedronate. For the synthesis of the ^{131}I-labeled risedronate with substitution at the 5-position of the pyridine ring, we designed a phased functional modification and radiolabeling strategy. The first step involves the synthesis of the radiolabeling precursor (compound **5**), which is divided into two main stages (Figure 1). The first stage is the construction of the bisphosphonate skeleton: starting with 5-bromo-3-pyridylacetic acid as the raw material, an acylation reaction was performed to generate the reactive intermediate (compound **2**). According to the method of Réjean Ruel and colleagues,[21] the acyl chloride undergone a Michaelis−Becker reaction with diethyl phosphite in the presence of the strong base KHMDS, yielding the esterified bisphosphonate intermediate (compound **3**).[22]

Compound **3** may undergo rearrangement side reactions under basic or heating conditions, resulting in byproduct **9** (Figure 3), which can be detected by ^{31}P NMR.[23] Multiple

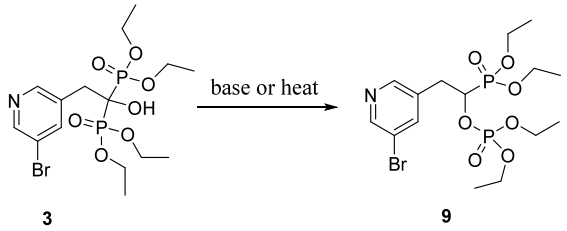

Figure 3. Rearrangement of diethyl 2-(5-bromopyridin-3-yl)-1-(diethoxyphosphoryl)-1-hydroxyethylphosphonate.

experiments revealed that low temperatures help maintain the structural stability of the target product. Although the formation of byproduct **9** is unavoidable, performing the reaction at low temperatures and quickly quenching it can reduce the proportion of rearranged product **9**. This byproduct can be removed by HPLC purification.

The second stage involves hydroxyl protection and the introduction of the tributyltin group. The reaction to convert bromine to a tributyltin group requires heating to 110 °C. To block the reactivity of the bisphosphonate hydroxyl group in subsequent reactions, the hydroxyl group of compound **3** was acetylated for protection, while also structurally preventing the molecule from undergoing rearrangement. Subsequently, the bromine atom at the 5-position of the pyridine ring was substituted with a tributyltin group through nucleophilic substitution using hexabutylditin reagents, resulting in the final radiolabeling precursor (compound **5**). In this molecular design, the acetylation of the hydroxyl group serves a dual purpose: it stabilizes the bisphosphonate backbone and prevents side reactions between the tributyltin group and the free hydroxyl group.

The next step involves the radioactive labeling of ^{131}I and deprotection of the protective groups (Figure 2), which is divided into three stages. The first stage is ^{131}I-labeling reaction: the tributyltin group of compound **5** was efficiently converted to ^{131}I in the presence of acetic acid, NCS, and [^{131}I]NaI,[24] resulting in the ^{131}I-risedronate derivative (compound **6**). The high reactivity of the tributyltin group ensures the specific incorporation of ^{131}I at the 5-position of the pyridine ring.

The second stage involves hydrolysis of the ethyl ester: it was found that for compound **6**, the traditional TMSBr/acetonitrile system requires heating to promote the reaction, but this easily leads to polymerization with solvent molecules, forming radiochemical impurities that are difficult to remove. By switching to TMSI reagent and performing hydrolysis under room temperature conditions,[25] the polymerization side reactions were successfully avoided. Solid-phase extraction was then used to enrich the product, yielding a high radiochemical purity de-esterified intermediate (compound **7**).

The last stage is deprotection of the acetyl group: compound **7** undergone hydrolysis in sodium hydroxide solution to remove the acetyl protection group, releasing the free hydroxyl group and yielding the final target product— ^{131}I-risedronate.

In choosing the labeling site, we selected the 5-position of the pyridine ring for ^{131}I covalent attachment to risedronate because this site maintains an appropriate distance from both the bisphosphonate group and the pyridine nitrogen atom, minimizing the impact of steric hindrance and electronic effects on bone-targeting properties. This labeling method not only preserves the drug's solubility and distribution coefficient but also significantly reduces the risk of radionuclide detachment through the stable covalent bond. In contrast, radionuclides such as ^{177}Lu and ^{153}Sm, which bind to bisphosphonates through coordination, carry the potential risk of radionuclide dissociation, which could lead to passive uptake in red bone marrow and cause radiation-induced damage.[26]

3.2. Biological Evaluation of ^{131}I-Risedronate. To evaluate the stability of ^{131}I-risedronate, a plasma stability study was conducted at 37%°C. As shown in Figure 4, ^{131}I-

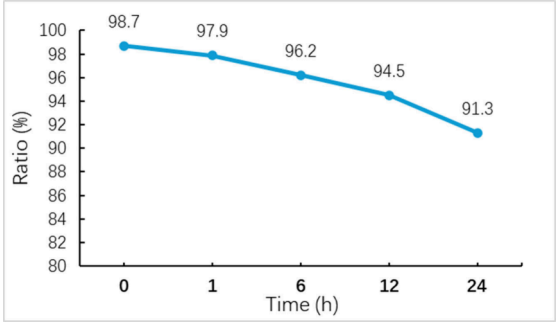

Figure 4. Plasma stability testing of ^{131}I-risedronate.

risedronate exhibited good radiochemical stability in plasma. The percentage of intact compound was 98.7% at 0%h and remained at 97.9% after 1%h. At 6%h and 12%h, the intact fraction was 96.2% and 94.5%, respectively. Even after 24%h of incubation, more than 90% (91.3%) of the radiolabeled compound remained intact, with free ^{131}I accounting for less than 9%. These results indicate that ^{131}I-risedronate possesses high stability under simulated physiological conditions, supporting its further application in biodistribution and imaging studies.

To systematically validate the biological characteristics of this molecule, we established a multidimensional experimental evaluation system. In the experimental design, we adopted a collaborative verification model combining biodistribution analysis and SPECT/CT imaging. Four time points were set: 1 h, 4 h, 1 day, and 3 days. At each time point, 4 normal BALB/c mice were selected for biodistribution testing to reduce experimental random errors. SPECT/CT imaging was performed at the same time points, utilizing the γ-rays emitted

https://doi.org/10.1021/acs.molpharmaceut.5c00300
Mol. Pharmaceutics 2025, 22, 3508−3514

Table 1. In Vivo Biodistribution of ^{131}I-Risedronate in Normal Mice (n = 4)

	%ID/g (S.D.)[a]			
tissue	1 h	4 h	1 day	3 days
femur	14.276 (5.49)	18.255 (8.183)	11.924 (1.275)	13.795 (2.025)
muscle	0.411 (0.215)	0.230 (0.287)	0.069 (0.024)	0.048 (0.010)
blood	1.158 (0.189)	0.659 (0.700)	0.154 (0.025)	0.077 (0.024)
intestine	0.493 (0.064)	0.366 (0.450)	0.100 (0.027)	0.078 (0.010)
stomach	2.518 (0.417)	0.972 (1.354)	0.098 (0.015)	0.077 (0.011)
heart	0.828 (0.074)	0.907 (1.060)	0.215 (0.068)	0.307 (0.282)
kidney	3.836 (0.495)	9.369 (14.804)	0.881 (0.085)	0.621 (0.067)

[a]Each value represents the mean (S.D.) for four animals.

during the decay of ^{131}I to visualize drug metabolism and track its distribution.

These two methods form a data feedback loop—biodistribution data provide quantitative radiological analysis of each organ, while SPECT/CT images visually present the spatial-temporal distribution characteristics of the drug. Combining both approaches allows for precise analysis of the bone-targeting kinetics of the molecule and its effects on other organs, enabling us to infer the potential and safety of this molecule for treating bone metastatic tumors.

The biodistribution results (Table 1) revealed the unique pharmacokinetic characteristics of the ^{131}I-risedronate molecule. The data indicate that this molecule has excellent bone-targeting efficiency: it is rapidly cleared from the bloodstream, and the distribution in nontarget tissues (such as muscle) remains extremely low (<0.5%ID/g) and continues to decrease over time, suggesting a low systemic exposure risk. Notably, the drug distribution in the femur peaks at 4 h postadministration and maintains a high retention level for up to 3 days (with the average always greater than 11%ID/g). This shows a significant advantage over other drugs such as ^{177}Lu-DOTA-IBA (only >11%ID/g at 3 days) and ^{177}Lu-DOTA-ZOL (always <4%ID/g).[8,27] In terms of metabolic pathways, the drug is primarily excreted via the kidneys. Radioactive accumulation in the kidney peaks at 4 h postadministration but rapidly decreases after 24 h, indicating a low renal exposure risk. The renal retention shows a time-dependent pattern, which is consistent with the typical metabolic behavior of small molecule drugs.

From the SPECT/CT images (Figure 5), the molecule shows significant bone uptake, with relatively low uptake in other organs. The contrast between the bone and other tissues is high, and the overall image resolution is clear, allowing for a detailed representation of the basic situation of bone. On day 3, the bone imaging remains relatively bright, while the radioactivity in other organs further decreases, consistent with the biodistribution results. Iodine has a unique affinity for the thyroid, but no significant radioactivity was observed in the thyroid region of the mice in the images, indicating that the ^{131}I is tightly bound to risedronate, with no radionuclide dissociation occurring.

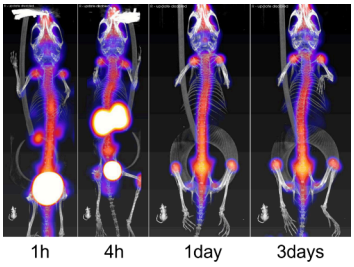

Figure 5. ^{131}I-risedronate SPECT whole-body static imaging in normal mice at different time points.

Previous studies have demonstrated that ^{131}I possesses relatively high safety. Its use in the treatment of thyroid cancer may be associated with a slight increase in the risk of second primary malignancies—approximately a 1% overall elevation, primarily involving leukemia and soft tissue sarcomas.[28,29] Conventional therapeutic ^{131}I is typically administered in free ionic form, which exhibits sustained distribution in the bloodstream, as shown by biodistribution data.[30] This prolonged circulation may increase radiation exposure to nontarget tissues.

In contrast, ^{131}I-risedronate covalently incorporates ^{131}I into its molecular structure and utilizes the bisphosphonate moiety to achieve high selectivity for bone tissue, ensuring high in vivo stability. It is rapidly cleared from the bloodstream and significantly reducing radiation exposure to normal tissues. In bone metastatic lesions, elevated bone metabolism leads to increased exposure of binding sites, promoting further accumulation of ^{131}I-risedronate. The β radiation emitted during the decay of ^{131}I can effectively damage and kill tumor cells within these metabolically active bone regions (Figure 6).

These results demonstrate the excellent bone-targeting ability of ^{131}I-risedronate, with a dual characteristic of bone tissue retention and rapid clearance from nontarget tissues. This not only ensures the required therapeutic window for radiotherapy but also reduces the risk of radiation toxicity and side effects, providing key safety evidence for subsequent clinical translation. This molecule has the potential to become a novel radiopharmaceutical for the treatment of bone metastatic tumors.

4. CONCLUSION

This paper presents a synthesis method for ^{131}I-risedronate for the treatment of bone metastatic tumors and the initial biological evaluation through SPECT/CT imaging and biodistribution testing in normal mice. The synthesis method demonstrated high reproducibility, ease of operation for radiolabeling, and a high radiochemical conversion rate, resulting in ^{131}I-risedronate with high purity. Animal experiments showed that the bone-targeting efficiency and SPECT/CT imaging quality of this molecule are significantly superior to existing drugs. It also exhibited a moderate retention time in bone, demonstrating potential as an economical, safe, universal, and efficient novel radiopharmaceutical for the treatment and companion diagnosis of bone metastatic tumors.

https://doi.org/10.1021/acs.molpharmaceut.5c00300
Mol. Pharmaceutics 2025, 22, 3508−3514

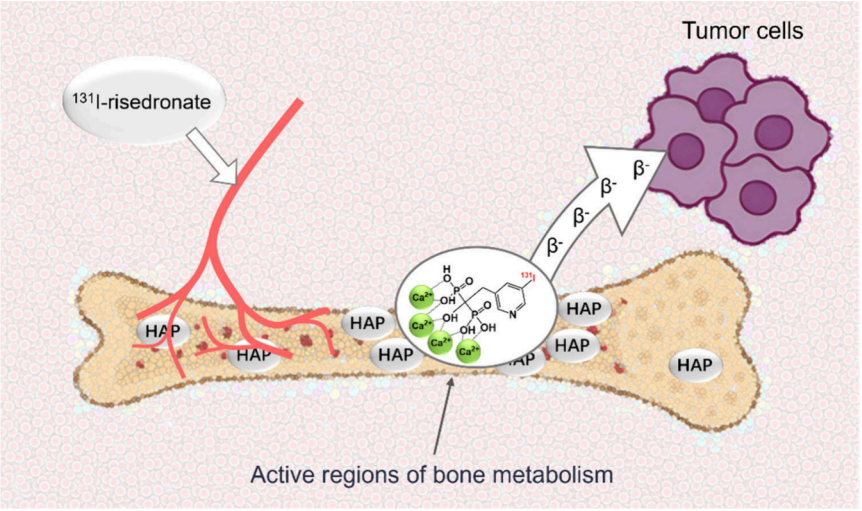

Figure 6. Mechanism of action of ^{131}I-risedronate.

Future experiments will focus on verifying the therapeutic efficacy of this drug, further evaluating its long-term safety, and assessing specific treatment regimens. It is expected that this drug will effectively control the progression of bone metastatic tumors and provide imaging-based tracking during treatment, improving the survival rate and quality of life for patients with bone metastatic tumors.

■ ASSOCIATED CONTENT

Supporting Information

The Supporting Information is available free of charge at https://pubs.acs.org/doi/10.1021/acs.molpharmaceut.5c00300.

Details on ^{1}H NMR spectra; ^{31}P NMR spectra; ^{13}C NMR spectra and HPLC analysis (PDF)

■ AUTHOR INFORMATION

Corresponding Authors

Jin-Hong Lin − *Department of Chemistry, College of Sciences, Shanghai University, Shanghai 200444, China; State Key Laboratory of Fluorine and Nitrogen Chemistry and Advanced Materials, Shanghai Institute of Organic Chemistry, University of Chinese Academy of Sciences, Chinese Academy of Sciences, Shanghai 200032, China;* orcid.org/0000-0002-7000-9540; Email: jlin@sioc.ac.cn, jlin@shu.edu.cn

Biao Li − *Department of Nuclear Medicine, Ruijin Hospital, Shanghai Jiao Tong University School of Medicine, Shanghai 200025, China*; Email: lb10363@rjh.com.cn

Ji-Chang Xiao − *State Key Laboratory of Fluorine and Nitrogen Chemistry and Advanced Materials, Shanghai Institute of Organic Chemistry, University of Chinese Academy of Sciences, Chinese Academy of Sciences, Shanghai 200032, China;* orcid.org/0000-0001-8881-1796; Email: jchxiao@mail.sioc.ac.cn

Authors

Zehui Lin − *Department of Chemistry, College of Sciences, Shanghai University, Shanghai 200444, China*

Wangxi Hai − *Department of Nuclear Medicine, Ruijin Hospital, Shanghai Jiao Tong University School of Medicine, Shanghai 200025, China;* orcid.org/0000-0003-0854-4590

Pengfei Pan − *State Key Laboratory of Fluorine and Nitrogen Chemistry and Advanced Materials, Shanghai Institute of Organic Chemistry, University of Chinese Academy of Sciences, Chinese Academy of Sciences, Shanghai 200032, China*

Complete contact information is available at: https://pubs.acs.org/10.1021/acs.molpharmaceut.5c00300

Author Contributions

‖Zehui Lin and Wangxi Hai contributed equally to this work

Notes

The authors declare no competing financial interest.

■ ACKNOWLEDGMENTS

The authors thank the Strategic Priority Research Program of the Chinese Academy of Sciences (XDB0590000), the National Natural Science Foundation of China (22271181), the National Key Research and Development Program of China (2021YFF0701700), the Science and Technology Commission of Shanghai Municipality (22ZR1423600), the Fundamental Research Funds for the Central Universities (No. YG2022QN005), and the construction project of Shanghai Key Laboratory of Molecular Imaging(18DZ2260400) for financial Support.

■ REFERENCES

(1) Cook, G. J. R. Imaging with radiolabelled bisphosphonates. *Bone* **2020**, *137*, 115372.

(2) Dyer, M. R.; Jing, Z.; Duncan, K.; Godbe, J.; Shokeen, M. Advancements in the development of radiopharmaceuticals for nuclear medicine applications in the treatment of bone metastases. *Nucl. Med. Biol.* **2024**, *130*−*131*, 108879.

(3) Bodei, L.; Lam, M.; Chiesa, C.; Flux, G.; Brans, B.; Chiti, A.; Giammarile, F. EANM procedure guideline for treatment of refractory metastatic bone pain. *Eur. J. Nucl. Med. Mol. Imaging* **2008**, *35* (10), 1934−1940.

(4) Kuroda, I. Effective use of strontium-89 in osseous metastases. *Ann. Nucl. Med.* **2012**, *26* (3), 197−206.

(5) Parker, C.; Nilsson, S.; Heinrich, D.; Helle, S. I.; O'Sullivan, J. M.; Fosså, S. D.; Chodacki, A.; Wiechno, P.; Logue, J.; Seke, M.; et al.

Alpha emitter radium-223 and survival in metastatic prostate cancer. *N Engl J. Med.* **2013**, *369* (3), 213−223.
(6) Turner, J. H.; Martindale, A. A.; Sorby, P.; Hetherington, E. L.; Fleay, R. F.; Hoffman, R. F.; Claringbold, P. G. Samarium-153 EDTMP therapy of disseminated skeletal metastasis. *Eur. J. Nucl. Med.* **1989**, *15* (12), 784−795.
(7) Maxon, H. R.; Thomas, S. R.; Hertzberg, V. S.; Schroder, L. E.; Englaro, E. E.; Samaratunga, R.; Scher, H. I.; Moulton, J. S.; Deutsch, E. A.; Deutsch, K. F.; et al. Rhenium-186 hydroxyethylidene diphosphonate for the treatment of painful osseous metastases. *Semin Nucl. Med.* **1992**, *22* (1), 33−40.
(8) Wang, Q.; Yang, J.; Wang, Y.; Liu, H.; Feng, Y.; Qiu, L.; Chen, Y. Lutetium177-Labeled DOTA-Ibandronate: A Novel Radiopharmaceutical for Targeted Treatment of Bone Metastases. *Mol. Pharmaceutics* **2023**, *20* (3), 1788−1795.
(9) Ferris, T.; Carroll, L.; Jenner, S.; Aboagye, E. O. Use of radioiodine in nuclear medicine-A brief overview. *J. Labelled Comp Radiopharm* **2021**, *64* (3), 92−108.
(10) Xue, Y. L.; Qiu, Z. L.; Song, H. J.; Luo, Q. Y. Value of ^{131}I SPECT/CT for the evaluation of differentiated thyroid cancer: a systematic review of the literature. *Eur. J. Nucl. Med. Mol. Imaging* **2013**, *40* (5), 768−778.
(11) Chinese Society of Nuclear Medicine Gao, Z.; Li, S. Guidelines for radioiodine therapy of differentiated thyroid cancer (2021 edition). *Chin J. Nucl. Med. Mol. Imaging* **2021**, *41* (4), 218−241.
(12) Geusens, P.; McClung, M. Review of risedronate in the treatment of osteoporosis. *Expert Opin Pharmacother* **2001**, *2* (12), 2011−2025.
(13) Nancollas, G. H.; Tang, R.; Phipps, R. J.; Henneman, Z.; Gulde, S.; Wu, W.; Mangood, A.; Russell, R. G.; Ebetino, F. H. Novel insights into actions of bisphosphonates on bone: differences in interactions with hydroxyapatite. *Bone* **2006**, *38* (5), 617−627.
(14) PetneháZy, I.; Jászay, Z. M.; Töke, L. Phosphite Addition to Carbonyl Group and Phosphoryl Migration Under Phase Transfer Catalytic Circumstances. *Phosphorus, Sulfur, and Silicon and the Related Elements* **1996**, *109* (1−4), 421−424.
(15) Russell, R. G.; Xia, Z.; Dunford, J. E.; Oppermann, U.; Kwaasi, A.; Hulley, P. A.; Kavanagh, K. L.; Triffitt, J. T.; Lundy, M. W.; Phipps, R. J.; et al. Bisphosphonates: an update on mechanisms of action and how these relate to clinical efficacy. *Ann. N.Y. Acad. Sci.* **2007**, *1117*, 209−257.
(16) Zheng, Y.; Zhou, H.; Dunstan, C. R.; Sutherland, R. L.; Seibel, M. J. The role of the bone microenvironment in skeletal metastasis. *J. Bone Oncol* **2013**, *2* (1), 47−57.
(17) Dougall, W. C. Molecular pathways: osteoclast-dependent and osteoclast-independent roles of the RANKL/RANK/OPG pathway in tumorigenesis and metastasis. *Clin. Cancer Res.* **2012**, *18* (2), 326−335.
(18) Dunn, C. J.; Goa, K. L. Risedronate: a review of its pharmacological properties and clinical use in resorptive bone disease. *Drugs* **2001**, *61* (5), 685−712.
(19) Wieland, D. M.; Wu, J.; Brown, L. E.; Mangner, T. J.; Swanson, D. P.; Beierwaltes, W. H. Radiolabeled adrenergi neuron-blocking agents: adrenomedullary imaging with [^{131}I]iodobenzylguanidine. *J. Nucl. Med.* **1980**, *21* (4), 349−353.
(20) William, B. M.; Bierman, P. J. I-131 tositumomab. *Expert Opin Biol. Ther* **2010**, *10* (8), 1271−1278.
(21) Ruel, R.; Bouvier, J.-P.; Young, R. N. Single-Step Preparation of 1-Hydroxybisphosphonates via Addition of Dialkyl Phosphite Potassium Anions to Acid Chlorides. *J. Org. Chem.* **1995**, *60*, 5209−5213.
(22) Lecouvey, M.; Leroux, Y. Synthesis of 1-hydroxy-1,1-bisphosphonates. *Heteroat Chem.* **2000**, *11* (7), 556−561.
(23) Nicholson, D. A.; Vaughn, H. A General Method of Preparation of Tetramethyl Alkyl-1-hydroxy-1,1-diphosphonates. *J. Org. Chem.* **1971**, *36* (24), 3843−3845.
(24) Chen, Y.; Foss, C. A.; Byun, Y.; Nimmagadda, S.; Pullambhatla, M.; Fox, J. J.; Castanares, M.; Lupold, S. E.; Babich, J. W.; Mease, R. C.; et al. Radiohalogenated prostate-specific membrane antigen (PSMA)-based ureas as imaging agents for prostate cancer. *J. Med. Chem.* **2008**, *51* (24), 7933−7943.
(25) Vachal, P.; Hale, J. J.; Lu, Z.; Streckfuss, E. C.; Mills, S. G.; MacCoss, M.; Yin, D. H.; Algayer, K.; Manser, K.; Kesisoglou, F.; et al. Synthesis and study of alendronate derivatives as potential prodrugs of alendronate sodium for the treatment of low bone density and osteoporosis. *J. Med. Chem.* **2006**, *49* (11), 3060−3063.
(26) Qiu, L.; Wang, Y.; Liu, H.; Wang, Q.; Chen, L.; Liu, L.; Wang, L.; Feng, Y.; Chen, Y. Safety and Efficacy of ^{68}Ga- or ^{177}Lu-Labeled DOTA-IBA as a Novel Theranostic Radiopharmaceutical for Bone Metastases: A Phase 0/I Study. *Clin Nucl. Med.* **2023**, *48* (6), 489−496.
(27) Meckel, M.; Bergmann, R.; Miederer, M.; Roesch, F. Bone targeting compounds for radiotherapy and imaging: *Me(III)-DOTA conjugates of bisphosphonic acid, pamidronic acid and zoledronic acid. *EJNMMI Radiopharm Chem.* **2017**, *1* (1), 14.
(28) Rubino, C.; de Vathaire, F.; Dottorini, M. E.; Hall, P.; Schvartz, C.; Couette, J. E.; Dondon, M. G.; Abbas, M. T.; Langlois, C.; Schlumberger, M. Second primary malignancies in thyroid cancer patients. *Br. J. Cancer* **2003**, *89* (9), 1638−1644.
(29) Sawka, A. M.; Thabane, L.; Parlea, L.; Ibrahim-Zada, I.; Tsang, R. W.; Brierley, J. D.; Straus, S.; Ezzat, S.; Goldstein, D. P. Second Primary Malignancy Risk After Radioactive Iodine Treatment for Thyroid Cancer: A Systematic Review and Meta-analysis. *Thyroid* **2009**, *19* (5), 451−457.
(30) Spetz, J.; Rudqvist, N.; Forssell-Aronsson, E. Biodistribution and Dosimetry of Free ^{211}At, ^{125}I- and ^{131}I- in Rats. *Cancer Biother Radiopharm* **2013**, *28* (9), 657−664.

https://doi.org/10.1021/acs.molpharmaceut.5c00300
Mol. Pharmaceutics 2025, 22, 3508−3514